Journal of Materials Chemistry B

ROYAL SOCIETY OF CHEMISTRY

PAPER

View Article Online
View Journal | View Issue

Cite this: J. Mater. Chem. B, 2025, 13, 8038

Immunomodulatory green nanomedicine production, tumor cellular targeting, *in vivo* biodistributions and preclinical therapeutic efficacy investigations of resveratrol-functionalized gold and theranostic ^{198}gold nanoparticles

Tamer M. Sakr,[ab] Velaphi C. Thipe,[bc] Kavita K. Katti,[bcd] Lisa Watkinson,[ef] Terry Carmack,[ef] Charles J. Smith,[efg] Cathy Cutler,[h] Prajna Hegde,[i] Anantkumar Hegde,[i] Ademar B. Lugão[j] and Kattesh V. Katti*[bcdgkl]

Prostate cancer remains a major global health concern demanding innovative therapeutic strategies. This study introduces a novel green nanotechnology approach for the development of a nanomedicine agent, also referred to as a nano-radiopharmaceutical, which integrates the antitumor and high antioxidant capacity of resveratrol phytochemical (RESV) with radioactive gold nanoparticles (^{198}AuNPs) for targeted prostate cancer therapy and diagnostics. The radioactive formulation, RESV–^{198}AuNP, was developed at the University of Missouri Research Reactor (MURR) using neutron-activated gold-198, which exhibited high radionuclidic and radiochemical purity. Stability testing in rat serum and saline demonstrated durability of up to 15 days. *In vivo* biodistribution studies in CF-1 mice and PC-3 tumor-bearing SCID mice have provided insights into pharmacokinetics and optimum tumor retention. Intratumoral administration of RESV–^{198}AuNP in SCID mice demonstrated strong retention within prostate cancer xenografts, suggesting tumor-specific uptake and retention. This study underscores the potential of RESV–^{198}AuNP as a dual-functional nano-radiopharmaceutical for prostate cancer theranostics. By combining resveratrol's anticancer properties with the therapeutic and imaging benefits of ^{198}AuNPs, this platform offers a promising avenue for improving treatment efficacy and enabling real-time therapeutic response monitoring. This research reveals the potential of RESV as a tumor-targeting agent and introduces a new perspective of green nanotechnology for dual anti-inflammatory radiosynovectomy as well as for use in cancer treatment. In-depth *in vivo* studies on the therapeutic efficacy of intratumorally administered RESV–^{198}AuNP revealed that over 85% of the injected dose (ID) remained within prostate tumors for up to 24 h. By the fourth week post-treatment, the treated group exhibited a greater than tenfold reduction in tumor volumes than the control group receiving saline. This study highlights emerging opportunities in green nanotechnology and introduces a clinically feasible approach to utilize resveratrol as a tumor-targeting agent in oncology, particularly for the application of RESV–^{198}AuNP in cancer treatments.

Received 8th April 2025,
Accepted 3rd June 2025

DOI: 10.1039/d5tb00815h

rsc.li/materials-b

[a] Radioactive Isotopes and Generator Department, Hot Labs Center, Egyptian Atomic Energy Authority, P. O. Box 13759, Cairo, Egypt
[b] Department of Radiology, School of Medicine, University of Missouri, Columbia, MO 65212, USA. E-mail: kattik@health.missouri.edu
[c] Institute of Green Nanotechnology, University of Missouri, Columbia, MO 65212, USA
[d] Indus University, Ahmedabad, Rancharda, Via, Shilaj, Gujarat 382115, India
[e] Harry S. Truman Memorial Veterans' Hospital, University of Missouri, Columbia, MO 65212, USA
[f] Molecular Imaging and Theranostics Center, University of Missouri, Columbia, MO 65212, USA
[g] University of Missouri Research Reactor (MURR), University of Missouri, Columbia, MO 65212, USA
[h] Isotope Research and Production Department, Brookhaven National Laboratory, Upton, NY 11973, USA
[i] Kadamba Intrac Private Ltd, Bangalore, KA 560011, India
[j] Instituto de Pesquisas Energéticas e Nucleares (IPEN), Comissão Nacional de Energia Nuclear-IPEN/CNEN-SP, São Paulo, SP, Brazil
[k] Department of Physics, University of Missouri, Columbia, MO 65212, USA
[l] Department of Biotechnology and Food Technology, University of Johannesburg, Doornfontein 2028, South Africa

Introduction

Prostate cancer (PCa) continues to persist as the second most prevalent malignancy among men worldwide, with metastatic progression to bone driving significant morbidity and mortality despite advances in therapeutic modalities.[1–3] Conventional interventions, including radical prostatectomy, chemotherapy, and external-beam radiotherapy, frequently fail to achieve durable remission owing to intrinsic chemoresistance, radioresistance, and the inability to control/eradicate micrometastases.[1] These challenges are compounded by the dense stromal architecture and molecular heterogeneity of primary tumors, which limit drug penetration and promote therapeutic escape.[4–6] Consequently, there is an urgent need for multifunctional platforms that integrate precision targeting, enhanced therapeutic payload delivery, and real-time monitoring capabilities.

Nanotechnology has emerged as a transformative paradigm in oncology, offering solutions to overcome the pharmacokinetic limitations of traditional chemotherapeutics and the off-target toxicity of radiotherapy.[7,8] Engineered and target-specific nanoparticles (NPs) exploit the dual capabilities of receptor-mediated targeting alongside enhanced permeability and retention (EPR) effects to preferentially accumulate diagnostic/therapeutic cargo within tumor microenvironments, while surface functionalization with tumor-specific ligands enables active targeting.[3,9–11] Among these innovations, gold nanoparticles (AuNPs) have garnered significant attention owing to their tunable surface chemistry, biocompatibility, and unique photophysical properties.[9] Our investigations, spanning over three decades, have shown that carefully engineered gold nanoparticles, functionalized with a myriad of targeting moieties, exhibit dual targeting and retention abilities within cancer cells.[4–7,12–20] We successfully utilize the high surface-area-to-volume ratios of gold nanoparticles to facilitate dense loading of therapeutic or diagnostic agents, while their sub-100 nm size permits efficient penetration across tumor cells/tissues, thus overcoming interstitial biological barriers.[15,19,21–24]

Radioactive AuNPs (^{198}Au) further exemplify the theranostic potential of these agents by combining beta radiation-mediated cytotoxicity with gamma emission-based scintigraphic imaging.[5,25–34] ^{198}Au qualifies as an excellent theranostic radioisotope because of its optimal physical properties. Au-198 has a beta particle emission (β_{max}) of 0.96 MeV, which allows a penetration depth of ~11 mm, thus enabling localized DNA damage while minimizing collateral toxicity. Most importantly, the ability to follow its biological distribution *via* its 412 KeV gamma-ray, along with a relatively short physical half-life of 2.7 days, ensures sustained tumor irradiation while providing unique dual therapeutic and diagnostic–theranostic advantages.[10,26] As most tumors manifest vascularity with pore sizes in the 300–500 nm range, engineered ^{198}AuNPs of up to 100 nm can accumulate in cancer cells owing to the irregularity of tumor vessels, large pore size, and poor lymphatic drainage (Scheme 1).[3,25] Preclinical studies in murine and canine models have demonstrated that intratumoral administration of ^{198}AuNP induces significant tumor regression and disease arrest while effectively suppressing metastatic dissemination, thus highlighting relatively unexplored clinical translatability of functionalized radioactive gold nanoparticles.[4,28,29,35–37]

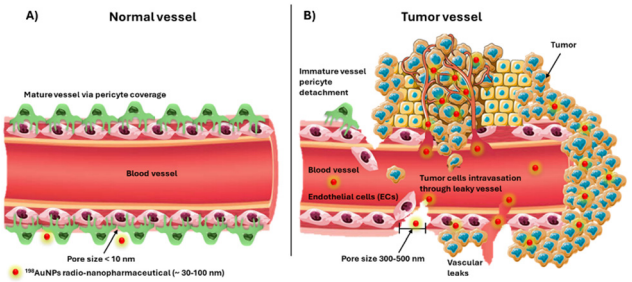

Scheme 1 Comparison of normal and tumor blood vessels, highlighting structural differences affecting drug delivery and cancer progression. (A) Normal vessels have intact pericyte coverage and small pores (<10 nm), restricting ^{198}AuNP extravasation. (B) Tumor vessels are immature, with detached pericytes, leaky endothelial cells, and large pores (300–500 nm), enabling ^{198}AuNP accumulation *via* EPR.

Complementing our long-standing green nanotechnology approaches in the design and development of nanomedicine agents,[4–7,12–20,27–29,33,34,36,38,39] our current work focuses on resveratrol (RESV; 3,5,4′-trihydroxy-*trans*-stilbene)—a natural polyphenol abundant in grapes and berries. Resveratrol exhibits multimodal anticancer activity through apoptosis induction, angiogenesis suppression, and sensitization of resistant PCa cells to radiotherapy.[40–45] However, RESV's clinical utility is constrained by rapid hepatic metabolism, poor aqueous solubility, and low tumor bioavailability.[43,46] Nanoencapsulation within lipid-based carriers (*e.g.*, solid lipid nanoparticles [SLNs] or biodegradable polymers, *e.g.*, PLGA–PEG) has shown some advantages in enhancing RESV stability, prolonging systemic circulation, and promoting tumor-selective delivery.[40,43,46,47] However, the constructive utility of RESV phytochemical, as a dual reducing agent and tumor specific capping moiety, to transform gold precursors into the corresponding gold nanoparticles, especially with the theranostic Au-198 gold precursor, has not yet been explored.

Nano-radiopharmaceuticals offer promising oncological approaches by combining the therapeutic and diagnostic capabilities of both nanoparticles and radioactive materials within singular platforms.[10,11,29,33,48] The synergistic integration of RESV with AuNPs presents a compelling strategy to amplify therapeutic efficacy. This phytochemical can radiosensitize tumor cells by modulating redox balance and DNA repair pathways, while 198-AuNPs serve as radiation dose enhancers and drug delivery vehicles.[2,19,44,49,50] We report, herein, the design, characterization, and preclinical evaluation of resveratrol-functionalized ^{198}AuNPs conjugate (RESV–^{198}AuNPs) engineered for targeted PCa nanotheranostics. We provide compelling experimental evidence on the mechanism(s) of action toward tumor retention and tumor specificity of RESV–^{198}AuNPs through detailed biodistribution studies in tumor-bearing PCa animal models. In addition, we provide full details of the therapeutic efficacy of the new RESV–^{198}AuNPs to highlight the realistic oncological potential of nano-radiopharmaceuticals for the treatment of various solid tumors in human patients.

Material and methods

Materials

All chemicals were of analytical grade and used directly without further purification unless otherwise stated. Sodium tetrachloroaurate ($NaAuCl_4$) (99.999%) and resveratrol (99% GC) were purchased from Sigma Aldrich Company (St Louis, MO). A gold foil target, 0.025 (0.001 in) thick and 99.985% basic metal, was purchased from the Alfa Aesar Company, MA, USA. DL-Cysteine (97% purity), bovine serum albumin (BSA), human serum albumin (HSA) in lyophilized form, sodium chloride (NaCl), phosphate-buffered saline (PBS), DAPI, MTT reagent, and trypan blue were procured from Sigma-Aldrich (St. Louis, MO, USA). Thermo Fisher Scientific (Waltham, MA, USA) supplied L-histidine (98% purity), gentamicin, and TrypLE Express solution. Fetal bovine serum (FBS), Roswell Park Memorial Institute (RPMI), and Dulbecco's modified Eagle medium (DMEM) culture media were obtained from Invitrogen Life Technologies (New York, NY, USA). Enzyme-linked immunosorbent assay (ELISA) Invitrogen kits (Tumour Necrosis Factor alpha (TNF-α) (88-7324), transforming growth factor beta 1 (TGF-β1) (88-8350), interleukin-1 beta (IL-1β) (88-7013), interleukin-6 (IL-6) (88-7064), interleukin-10 (IL-10) (88-7105), and interleukin-12 p70 (IL-12) (88-7121)) were obtained from Thermofisher Scientific (Waltham, MA, USA). Milli-Q water was used for all solution preparations. The prostate cancer cell line (PC-3), murine macrophages (RAW 264.7), and human aortic endothelial cell line (HAEC) were acquired from the American Type Culture Collection (ATCC, Manassas, VA, USA).

Synthesis of non-radioactive resveratrol-functionalized gold nanoparticles (RESV–AuNP)

Synthesis of RESV–AuNP was carried out using the method described by Thipe *et al.*[19] Briefly, 2 mg of resveratrol was dissolved in 6 mL of deionized water, and the solution was stirred at room temperature for 10 min. Subsequently, 100 mL of 0.1 M $NaAuCl_4$ prepared in deionized water was added to the solution under continuous stirring. The synthesis of AuNPs was validated by observing a color shift in the solution from yellow to deep ruby red. Characterization was performed using techniques such as UV-vis absorption spectroscopy, particle size analysis, transmission electron microscopy (TEM) and scanning transmission electron microscopy coupled with energy-dispersive X-ray spectroscopy (STEM-EDX).

In vitro stability of RESV–AuNP

The stability of RESV–AuNP under *in vitro* conditions was evaluated by exposing them to various biological media, including 0.5% bovine serum albumin (BSA), 0.5% human serum albumin (HSA), 0.5% cysteine, 0.2 M histidine, 1% sodium chloride (NaCl), RPMI and DMEM cell culture media, and phosphate-buffered saline (PBS) adjusted to pH 5, 7, and 9. For the assay, 200 mL of RESV–AuNP was combined with 800 mL of each test solution in 1.5 mL microcentrifuge tubes. The mixtures were incubated for 24 h in a 5% CO_2 incubator at 37 °C. Changes in nanoparticle stability were assessed by monitoring shifts in the surface plasmon resonance (SPR) peak using UV-vis absorption spectroscopy.

Cellular internationalization of RESV–AuNP by TEM and STEM-EDX

PC-3 and HAEC cells were seeded into six-well plates at a density of 8×10^5 cells per mL and maintained under standard culture conditions. After rinsing with 1× phosphate-buffered saline (PBS), the cells were treated for 24 h at 37 °C with a culture medium containing RESV–AuNP at a concentration of 50 μg mL^{-1}. After incubation, the cells underwent PBS washing and were detached using TrypLE Express reagent for 3 min. The enzymatic reaction was neutralized by adding fresh medium, after which the cell suspension was transferred to 1.5 mL microcentrifuge tubes. Centrifugation at 1000 rpm for 5 min pelleted the cells, followed by washing several times with PBS.

For ultrastructural preservation, cell pellets were fixed with a 2% glutaraldehyde and 2% paraformaldehyde solution prepared in 0.1 M sodium cacodylate buffer. Secondary fixation was performed using 1% osmium tetroxide combined with 2-mercaptoethanol. Sequential dehydration steps employed increasing acetone gradients (50–100%), after which the samples were embedded in Epon-Spurr epoxy resin. Ultrathin sections (85 nm thickness) were prepared with a diamond knife (Diatome, Hatfield, PA) and mounted for staining. Tissue sections underwent dual contrast with Sato's triple lead stain and 5% uranyl acetate in an aqueous solution. Imaging was conducted at the University of Missouri-Columbia's electron microscopy core using a JEOL JEM-1400 TEM (JEOL, Peabody, MA) operated at 80 kV accelerating voltage and a Spectra 300 STEM (ThermoScientific, Waltham, MA) for elemental mapping operated at 200 kV with a spot size of 8.

Immunomodulatory effect of RESV–AuNP on RAW 264.7 macrophage cells

RAW 264.7 murine macrophage cells were cultured in DMEM supplemented with 10% fetal bovine serum and gentamicin and maintained at 37 °C in a humidified atmosphere containing 5% CO_2. For the experiment, cells were seeded in multi-well plates at a density ensuring 70–80% confluency the following day. Cells were then pre-treated with RESV––AuNP at a concentration of 50 μg mL^{-1} for one hour to facilitate cellular internalization of the nanoparticles. After the pre-treatment period, lipopolysaccharide (LPS) was added at a final concentration of 1 μg mL^{-1}, and the cells were incubated for an additional 4 hours to induce an inflammatory response. Following incubation, the supernatants were carefully collected, centrifuged at low speed to remove any cellular debris, and stored at −80 °C until cytokine analysis. Levels of pro- and anti-inflammatory cytokines (IL-1β, TNF-α, TGF-β1, IL-6, IL-10, and IL-12) were quantified using enzyme-linked immunosorbent assay (ELISA) kits according to manufacturing protocols. Standard curves were generated for each cytokine, and the optical densities were measured at 450 nm using a calibrated SpectraMax M2 microplate reader (Molecular Devices LLC, San Diego, CA, USA), ensuring that all samples and standards were run in triplicate to guarantee statistical reliability. The data were normalized to

untreated controls, and the results were analyzed to assess the modulatory effects of RESV–AuNP on LPS-induced cytokine production.

Synthesis of radioactive resveratrol-functionalized gold nanoparticles (RESV–^{198}AuNP)

The production of non-radioactive RESV–AuNPs, typically done *via* simple chemical reduction, is far less complex than that of the radioactive RESV–^{198}AuNP counterpart. Radioactive nanoparticles require neutron activation in a nuclear reactor, strict radiation safety, and regulatory compliance. These added steps make radioactive nanoparticle synthesis far more challenging and resource intensive, as demonstrated below.

Gold-198 (^{198}Au) production, QA and QC

The isotope ^{198}Au prepared by neutron irradiation of natural gold foil *via* a direct neutron capture nuclear reaction at the Missouri University Research Reactor (MURR) is represented by the following equation: ^{197}Au(n,γ)^{198}Au. In the synthesis of RESV–^{198}AuNP, neutron activation was carried out using a thermal neutron flux of approximately 8×10^{13} neutrons cm^{-2} s^{-1} for 6 to 40 h using 5–30 mg of gold foil, resulting in an initial activity concentration of approximately on average 0.5–1 mCi mg^{-1} immediately post-irradiation. After irradiation, the activated foil was dissolved in 400 mL of aqua regia, followed by heating to reduce the solution to a near-dry state. To remove residual nitric acid, 400 mL of 0.05 M HCl was added in three successive aliquots, each followed by azeotropic distillation under heating. The radionuclidic and radiochemical purity of ^{198}Au was checked by HpGe spectroscopy and Radio-TLC, as shown in Scheme 2.

All measurements reported were decay-corrected to the time of administration using the known half-life of ^{198}Au (2.7 days). The administered dose was carefully adjusted to deliver approximately 136 μCi per injection.

Resveratrol-^{198}AuNP (RESV–^{198}AuNP) preparation

Synthesis of RESV–^{198}AuNP was carried out using the method described by Thipe *et al.*[19] with a modified protocol, as the radioactive gold precursor was prepared by combining a total gold mass (radioactive ^{198}Au + non-radioactive Au) of 1.477 mg, where the proportion of ^{198}Au was based on the final desired amount of radioactivity. We prepared ^{198}Au/NaAuCl$_4$ with activity concentrations of up to 1 mCi mL^{-1}.

Characterization of radioactive gold nanoparticles (RESV–^{198}AuNP)

The following instrumentation was used to fully characterize the RESV–^{198}AuNPs used in these investigations: AR-2000 Radio-TLC Imaging Scanner, Eckert & Ziegler; Radiopharma, Bioscan Inc., Berlin, Germany; Atomlab 100 Dose Calibrator; Biodex Medical System Inc., New York, USA; and ISS-UV-vis Integrated Sampling System, Ocean Optics Inc., Florida, USA. The morphology and size distribution of RESV–^{198}AuNPs were determined using TEM.

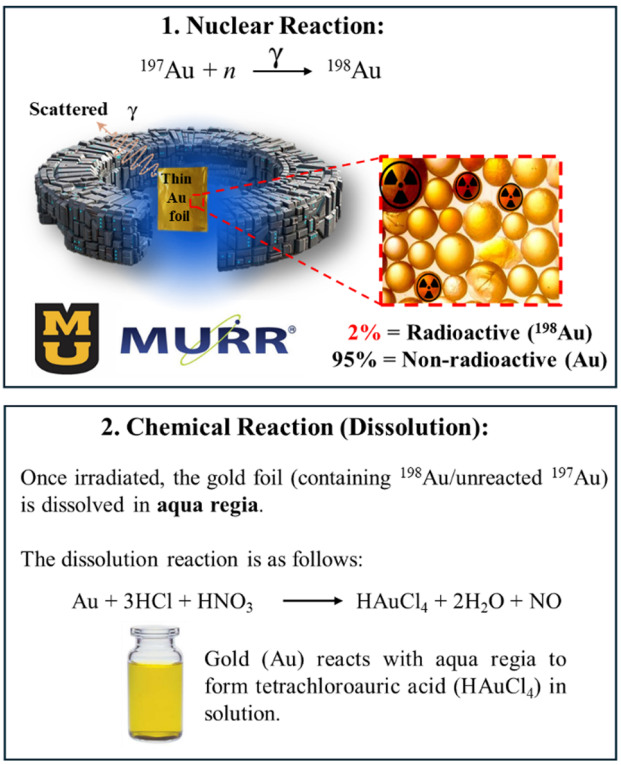

Scheme 2 Production scheme for ^{198}Au *via* neutron irradiation at the MURR.

Quality control of radioactive gold nanoparticles (RESV–^{198}AuNP)

RESV–^{198}AuNP UV absorbance. The UV-vis absorbance of RESV–^{198}AuNP was measured using Ocean optics instrumentation after diluting 200 mL aliquots of the radiotracer in 600 mL of H_2O.

RESV–^{198}AuNP UV radiochemical purity. The radiochemical purity of RESV–^{198}AuNP was determined by TLC, where 1 mL aliquots were spotted on the TLC plates and then developed in a mixture of methanol and concentrated HCl. Once they were dry, they were scanned using Bioscan 2000.

RESV–^{198}AuNP UV particle size. After the complete decay of radioactivity, the particle core diameter was checked using a transmission electron microscope (TEM).

In vitro stability of radioactive gold nanoparticles (RESV–^{198}AuNP)

The *in vitro* stability of the RESV–^{198}AuNP was tested at room temperature in rat serum and in saline. The *in vitro* stability of the RESV–^{198}AuNP was evaluated for up to 15 days by mixing 450 mL of rat serum or saline with 50 mL of RESV–^{198}AuNP.

In vivo biodistribution studies of RESV–^{198}AuNP

The biodistribution studies of RESV–^{198}AuNP were evaluated in normal female CF-1 mice and PC-3 tumor-bearing SCID mice (Charles River Laboratories, NY, USA). All animal studies were conducted in compliance with the highest standards of care as outlined in the NIH Guide for the Care and Use of Laboratory

Animals (8th edn) and the Policy and Procedures for Animal Research at the Truman VA Hospital, Columbia, Missouri, USA. All the animal investigations performed herein were approved by the Subcommittee for Animal Safety at the Truman VA Hospital, Columbia, Missouri, USA and the University of Missouri IACUC, Columbia, Missouri, USA. Male CF-1 mice aged 4–5 weeks were used for this series of investigations.

Biodistribution studies of RESV–^{198}AuNP on normal murine models

A cohort of 25 normal female CF-1 mice (5 animals per experimental group) received an intravenous (IV) administration of 5.0 mCi/100 mL of RESV–^{198}AuNPs *via* the tail vein. Animals were humanely euthanized at sequential time intervals (0.5, 1, 2, 4, and 24 h post-injection), and tissues of interest, including the heart, liver, spleen, lungs, skeletal muscle, bladder, brain, bone, kidneys, gastrointestinal tract, blood, and stomach, were harvested, weighed, and analyzed for radioactivity accumulation. Tissue samples and calibration standards were quantified using a sodium iodide (NaI) well counter. Radioactive counts were normalized to the injected dose and expressed as both the percentage of injected dose per organ (%ID) and the percentage of injected dose per gram of tissue (%ID per g). Whole-blood radioactivity was calculated under the assumption that blood volume constitutes 6.5% of total body mass based on established murine physiological parameters. As a measure of nanoparticle stability, minimal accumulation of radioactivity in highly perfused tissues (*e.g.*, blood and lungs) was anticipated.

Biodistribution and tumor retention (intratumoral delivery) studies of RESV–^{198}AuNPs on severe combined immunodeficiency (SCID) murine models

Severe combined immunodeficiency (SCID) mice were administered unilaterally *via* subcutaneous injection in the hind flank with 10×10^6 PC-3 cells suspended in 0.1 mL of sterile DPBS mixed with Matrigel® at a 2 : 1 (v/v) ratio under inhaled anesthesia (a mixture of isoflurane and oxygen). Tumor growth was permitted for four weeks to establish solid xenografts. Subsequently, a single intratumoral dose of RESV–^{198}AuNPs (4 mCi in 30 mL per tumor) was administered directly into the prostate tumor. Cohorts of mice ($n = 5$ per time point) were euthanized at predetermined intervals (0.5, 1, 2, 4, and 24 h post-injection). Target organs and tumors were dissected, weighed, and analyzed alongside calibration standards using a NaI gamma well counter. Tissue radioactivity was quantified as the percentage of injected dose (%ID) and normalized to organ mass (%ID per g).

Therapeutic efficacy investigations of RESV–^{198}AuNP

In this study, a prostate cancer model was established using female SCID mice. The SCID mice were subcutaneously injected with a mixture of PC-3 cells, Matrigel®, and sterile DPBS into the right hind flank of each mouse under isoflurane anesthesia. After a 4-week tumor growth period, during which tumor volumes were regularly measured using a digital caliper, the mice were randomly divided into two groups. The day of randomization was designated as day 0 for the therapy study. On day four, the treatment protocol was implemented. The control group received an intratumoral injection of sterile DPBS, while the treatment group was given a single intratumoral dose of RESV–^{198}AuNP (160 μCi/30 μL). This experimental design allowed for the evaluation of the therapeutic potential of RESV–^{198}AuNP in treating prostate cancer *in vivo*, considering different tumor sizes and comparing the results against a control group.

Statistical analysis

The data, unless otherwise specified, were estimated as an average of three replicates. A *p*-value of less than 0.05 from the one-way ANOVA test indicated a statistically significant result. All statistical tests were performed using GraphPad Prism v9.0.

Results and discussion

Characterization of non-radioactive and radioactive RESV–AuNP

RESV–^{198}AuNPs were synthesized using an adapted protocol originally developed for their non-radioactive RESV–AuNP counterparts.[19] Prior to radiolabeling, the procedure was rigorously optimized to ensure reproducibility from the non-radioactive formulation. The synthesis involved the direct mixing of resveratrol with gold salt in aqueous media, where the inherent electron-rich properties of resveratrol facilitated the efficient reduction of the gold precursor, yielding RESV–AuNPs with high purity with minimal/no aggregation (Fig. 1).

The structural and morphological properties of RESV–AuNPs were characterized using UV-vis spectroscopy and advanced microscopy. TEM analysis revealed spherical, monodisperse nanoparticles with a core diameter of 23 ± 3 nm (Fig. 2). Dynamic light scattering (DLS) measurements further demonstrated a hydrodynamic diameter of 58 ± 0.9 nm and a zeta potential of −35 ± 1.1 mV (Table 1). The disparity between the core (20 nm) and hydrodynamic diameter (58 nm) confirms successful resveratrol encapsulation, forming a stable surface coating. The pronounced negative zeta potential (−35 mV) indicates strong electrostatic repulsion between particles, which is critical for colloidal stability and resistance to agglomeration under physiological conditions. This robust stability profile underscores the suitability of RESV–AuNPs for long-term *in vitro* and *in vivo* applications.

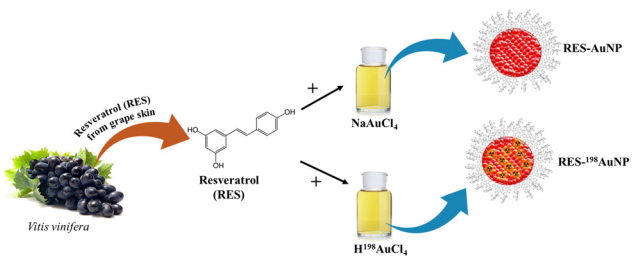

Fig. 1 Schematic representation of using resveratrol (3,5,4′-trihydroxy-*trans*-stilbene) for the production of RESV–AuNP and RESV–^{198}AuNP.

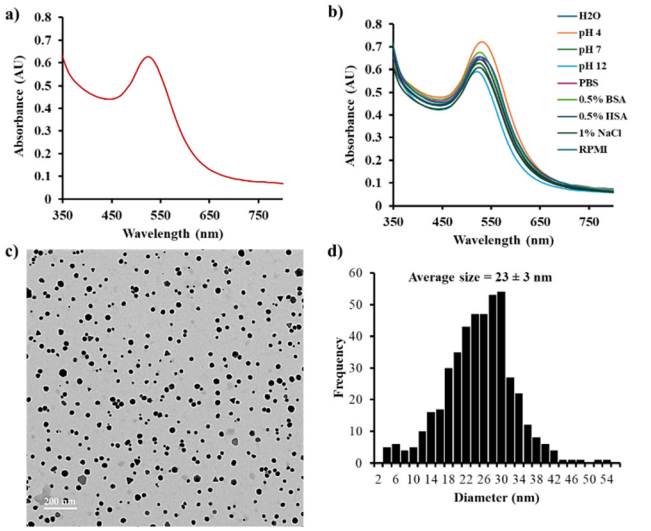

Fig. 2 Characteristic profile of RESV–AuNP: (a) UV-Visible spectrum; (b) UV-Vis spectra showing the *in vitro* stability of RESV–AuNP in biological solutions; (c) TEM image, scale bar: 200 nm and (d) size distribution histogram.

Table 1 Physiochemical data parameters of RESV–AuNP

UV-Vis SPR peak (nm)	Hydrodynamic size (nm)	Zeta potential (mV)	PDI	Core size (nm)
535	58 ± 0.9	−35 ± 1.1	0.2	23 ± 3

Note. SPR: surface plasmon resonance and PDI: polydispersity index.

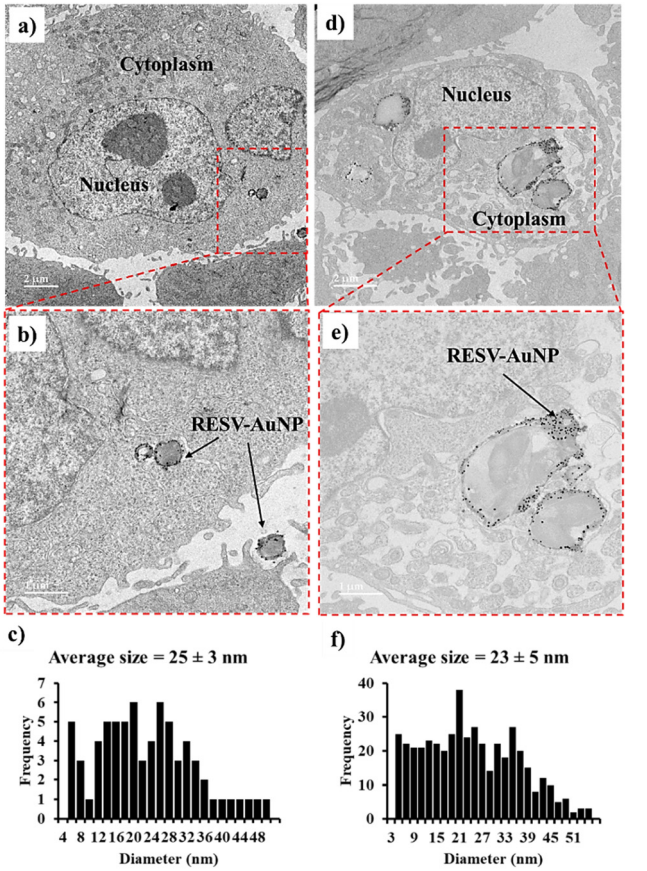

Fig. 3 TEM images showing the cellular internalization of RESV–AuNP in HAEC cells (a) and (b) and PC-3 cells (d) and (e). Size distribution histograms of internalized RESV–AuNP in HAEC (c) and preferential accumulation in PC-3 cells (f).

Cellular internationalization of RESV–AuNP by TEM

TEM images provide a comparative analysis of the internalization of RESV–AuNP in HAEC and PC-3 cells. In HAEC, RESV–AuNP uptake is limited, with several nanoparticles remaining outside the cells, as shown in Fig. 3a and b. This suggests that HAEC lacks cell surface receptors and vascularity, thus exhibiting the lowest affinity for RESV–AuNPs. This is significant to minimize off target toxicity of RESV–AuNPs on normal cells. Conversely, PC-3 cells exhibited significantly higher RESV–AuNP internalization attributable to higher resveratrol-specific tumor-specific receptor density. The dual interplay of EPR effects as well as the overexpression of RESV–AuNP-specific receptors in PC-3 cells account for the significantly higher therapeutic loads of RESV–AuNP in prostate tumor cells (Fig. 3d and e). The EPR effect is a well-documented phenomenon in tumor biology, where the leaky vasculature of tumors facilitates the passive accumulation of RESV–AuNP while impaired lymphatic drainage prevents their clearance.[25] This contributes to the selective retention of RESV–AuNP within the tumor microenvironment. Additionally, receptor-mediated endocytosis plays a crucial role in the preferential uptake of RESV–AuNP by PC-3 cells. Cancer cells often overexpress specific receptors, such as folate, transferrin, and integrins, which enhance AuNP binding and internalization. The significant presence of RESV–AuNP in PC-3 cells suggests that functionalization with RESV promotes targeted uptake. The size distribution of the RESV–AuNP in HAEC and PC-3 cells is 25 ± 3 nm and 23 ± 5 nm, respectively. The well-preserved size of the RESV–AuNP signifies their stability within the intricate cellular environment. This stability highlights the potential of RESV–AuNP as a targeted therapeutic agent for tumor cells, offering minimal toxicity to healthy tissues.

STEM EDX analysis of RESV–AuNP in PC-3 cells

STEM-EDX analysis was conducted at 200 kV to characterize the sample. As shown in Fig. 4a, the dark-field image reveals bright spots corresponding to gold nanoparticles. Energy-dispersive spectroscopy (EDS) mapping, performed at a resolution of 25 nm, confirmed the localization of gold. Fig. 4b displays the EDS spectra with distinct gold L-line peaks, verifying the intracellular presence of gold nanoparticles corroborating the data from the TEM cellular internalization studies.

Immunomodulatory activity of RESV–AuNP on RAW 264.7 macrophage cells

Across the cytokine panels (Fig. 5), RESV–AuNP-treated RAW 264.7 macrophages exhibited a distinctive pattern of down-regulated proinflammatory IL-1β, IL-6, IL-10, and TGF-β1 levels, while concomitantly upregulating anti-inflammatory IL-12 and

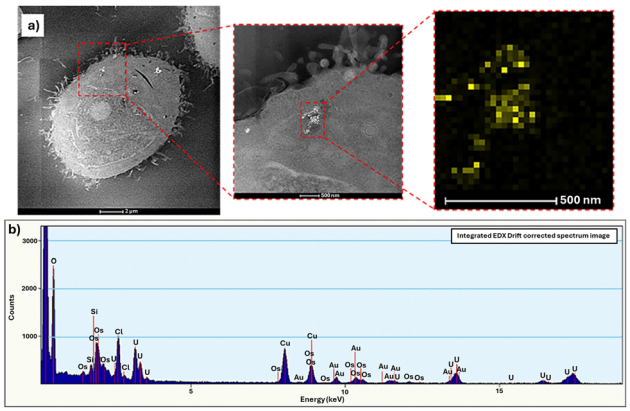

Fig. 4 Cellular internalization and elemental mapping of RESV–AuNP in PC-3 cells. (a) Dark-field image of PC-3 cells treated with RESV–AuNP and (b) EDS spectra confirming the presence of gold in the cells.

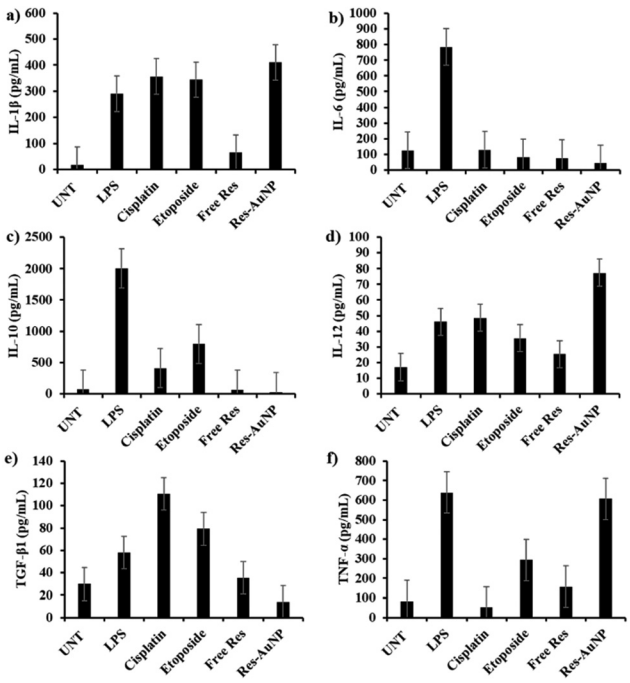

Fig. 5 Immunomodulatory effects of RESV–AuNP on RAW 264.7 macrophage cells compared with lipopolysaccharide (LPS), cisplatin, and etoposide treatment strategies. Each panel (a)–(f) represents the mean ± SD (n = 3) of key cytokine levels measured under different treatment conditions: (a) IL-1β, (b) IL-6, (c) IL-10, (d) TGF-β1, (e) IL-12 and (f) TNF-α.

TNF-α levels, in comparison to LPS-, cisplatin-, and etoposide-treated cells. These specific cytokine profiles are significant for several reasons. First, IL-1β and IL-6 are typically associated with robust pro-inflammatory responses, but they can also contribute to chronic inflammation and tumor progression if excessively elevated. By keeping IL-1β and IL-6 at relatively lower levels, RESV–AuNP may help mitigate detrimental hyperinflammation while still harnessing enough pro-inflammatory capacity for anti-tumor effects. Similarly, the reduction of IL-10 and TGF-β1, two potent immunosuppressive cytokines, suggests that RESV–AuNP can dampen pathways often exploited by tumor cells to evade immune surveillance. Lower IL-10 and TGF-β1 levels generally favor a shift away from an immunosuppressive (M2-like) macrophage environment, thereby promoting anti-tumor immunity.

Concurrently, the observed upregulation of IL-12 and TNF-α by RESV–AuNP points to the enhanced capacity of macrophages to foster a Th1-type immune response, which is widely recognized for its tumoricidal properties. IL-12 stimulates cytotoxic T-lymphocyte (CTL) activity and helps coordinate a cell-mediated immune response, while TNF-α can directly induce tumor cell apoptosis and further amplify inflammatory signaling. Compared to the effects of LPS, known for triggering a more generalized "hyper-activation" of macrophages, RESV–AuNP appears to steer macrophages toward a more selective, therapeutically favorable cytokine profile. Meanwhile, in comparison to the cytotoxic drugs cisplatin and etoposide, RESV–AuNP bolsters immune-mediated tumor-killing mechanisms without incurring the broader immunosuppressive side effects frequently associated with traditional chemotherapy. Taken together, these findings highlight RESV–AuNP's potential to fine-tune macrophage function, strike a balance between sufficient pro-inflammatory activity and controlled immunomodulation, and ultimately strengthen the innate immune system's capacity to combat tumor cells. These findings further support our new green nanotechnology-based drug design for the creation of immunomodulatory RESV–AuNPs for use as immunotherapeutic or immunoadjuvant therapeutic strategies. It is important to recognize that RESV–AuNPs can be advantageously used in combination therapies to mitigate the immunocompromising effects associated with most chemotherapeutic or radiotherapeutic agents.

Gold-198 (^{198}Au) production

Gold-198 was successfully produced with 99.99% radionuclidic purity according to HPGe detection and with 99% radiochemical purity, as determined by TLC.

RESV–^{198}AuNP preparation and QC

RESV–^{198}AuNPs were successfully prepared with high radiochemical purity (97%) in reproducible batches, as confirmed by Radio-TLC (Fig. 6). The surface plasmon resonance wavelength (λ_{max}) was at 540 nm, confirming their formation, as shown in Fig. 6. TEM revealed an average core size distribution of 29 ± 7 nm. Collectively, these data show similar physicochemical properties corresponding to non-radioactive RESV–AuNPs (Fig. 4 and Table 1).

It is important to recognize that the perceived heterogeneity in particle presentation is a function of image scale and magnification, not variability in the formulation. The nanoparticle system demonstrates consistent size, shape, and dispersion, validated through TEM and UV-vis analyses for both radioactive and non-radioactive samples. These results collectively confirm the homogeneity and reproducibility of our RESV–AuNP and RESV–^{198}AuNP systems.

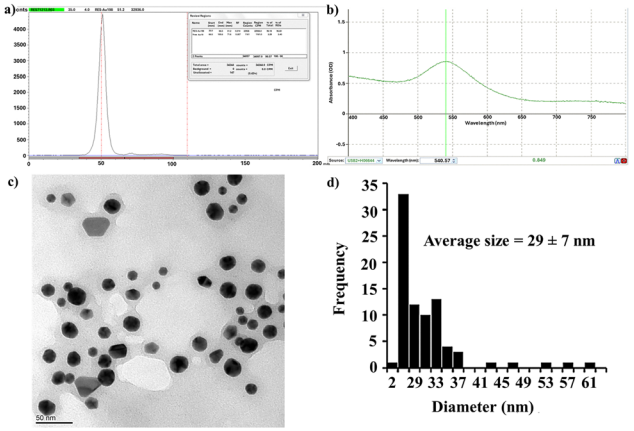

Fig. 6 Physiochemical characteristics of (a) TLC radiochromatogram; (b) UV-vis spectrum; (c) TEM image, scale bar: 50 nm; and (d) size distribution of radioactive RESV–^{198}AuNP.

RESV–^{198}AuNP *in vitro* stability

To assess the *in vivo* stability, tumor targeting, and biodistribution of radioactive RESV–^{198}AuNP in animal models, it is essential to adjust the pH of the sample to physiological pH. This adjustment is crucial because AuNPs are highly sensitive and prone to aggregation and precipitation when exposed to pH changes. RESV–^{198}AuNPs showed *in vitro* stability for up to 4 days in rat serum and saline, as monitored by UV-vis λ_{max} SPR and Radio-TLC profiles over time. The *in vitro* stability of RESV–^{198}AuNP was comparable to that of non-radioactive RESV–AuNPs. These *in vitro* stability results provide impetus for further *in vivo* investigations of the biodistribution, tumor specificity, and therapy of RESV–^{198}AuNP.

Biodistribution studies of RESV–^{198}AuNP

To function effectively as diagnostic and therapeutic agents, AuNPs must maintain stability *in vivo*, minimizing or avoiding interactions with blood plasma proteins while exhibiting strong resistance to aggregation. The accumulation of AuNPs in specific organs following *in vivo* administration in animal models serves as a key indicator of their stability. Stable AuNPs are generally characterized by low levels of blood uptake and higher levels of liver accumulation, as they are typically cleared *via* the hepatobiliary pathway. Conversely, instability *in vivo* is evident when AuNPs exhibit significant blood accumulation, which can result from surface interactions with serum proteins or aggregation into larger particles that accumulate in the blood and lungs. To evaluate the *in vivo* stability of RESV–^{198}AuNP, we conducted a comprehensive biodistribution study in normal mice.

Our study focused on conducting biodistribution experiments of RESV–^{198}AuNPs in healthy mice to quantitatively determine the concentration of gold in various organs at specific time intervals (0.5, 1, 2, 4, and 24 h) following IV administration. At each time point, five mice (n = 5) were euthanized, and their organs were promptly collected, weighed, and analyzed for ^{198}Au radioactivity using a NaI scintillation counter alongside appropriate standards. The results, as shown in Fig. 7, illustrate the biodistribution of RESV–^{198}AuNPs across different organs as the average percentage of the injected dose per gram (%ID per g) for each organ. The results showed an initial average uptake of 55.63 ± 4.48 and 63.95 ± 26.66%ID per g at 30 min in the liver and spleen, which increased to 61.47 ± 8.14 and 69.8 ± 33.12%ID per g at 24 h, respectively. The minimal uptake of RESV–^{198}AuNP in the lung and blood was relatively low at 3.24 ± 0.54%ID per g and 1.61 ± 0.49%ID per g at 0.5 h, decreasing to 1.94 ± 0.24%ID per g and 0.61 ± 0.37%ID per g at 24 h, respectively. Other organs, such as the kidneys, heart, and brain, showed minimal accumulation at less than 2%ID per g. This low accumulation in these organs suggests a reduced potential for off-target effects in these tissues, thus confirming the *in vivo* stability of RESV–^{198}AuNP.

The *in vivo* stability data obtained thus far have been promising. Recent studies, including our own, have demonstrated that polyphenol-functionalized AuNPs effectively target laminin receptors.[19] Based on this, we hypothesized that the strong affinity of polyphenolic RESV for laminin receptors, which are abundant in prostate tumor cells, would exhibit enhanced tumor uptake, as illustrated in Fig. 3, and thus could improve the retention of RESV–^{198}AuNP in prostate tumors. Validating this hypothesis experimentally could pave the way for a new class of prostate tumor-specific diagnostic and therapeutic nanoceuticals using RESV–^{198}AuNP.

The pharmacokinetics of RESV–^{198}AuNP retention and clearance from tumor sites are critical, as these factors determine the therapeutic payload's effectiveness in tumor treatment. Nanoparticles exhibiting high tumor retention with minimal leakage enhance therapeutic efficacy and reduce the potential toxic effects associated with radiation damage to non-target organs. To investigate this, we conducted *in vivo* experiments to

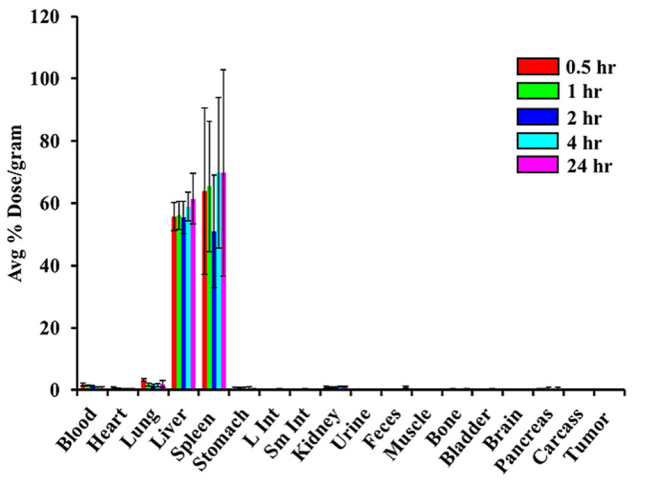

Fig. 7 Biodistribution profile of RESV–^{198}AuNPs in normal CF-1 female mice following a single intravenous tail vein injection (5.0 mCi/100 mL). Radioactivity levels were assessed at 0.5, 1, 2, 4, and 24 h post-injection and expressed as a percentage of the injected dose per gram (%ID per g) for each organ.

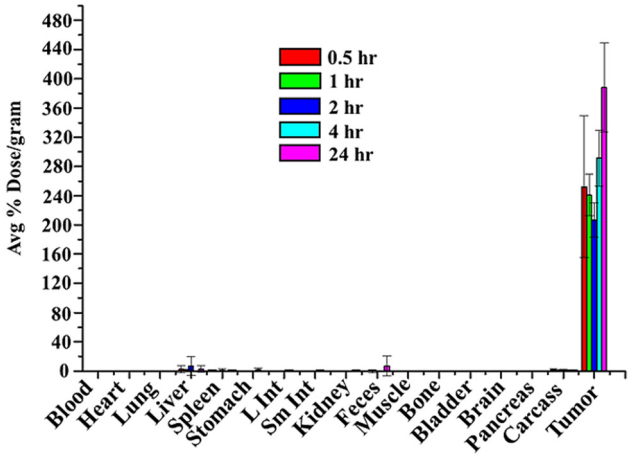

Fig. 8 Biodistribution profile of RESV–^{198}AuNPs in a PC-3 tumor-bearing SCID mice model following a single intravenous tail vein injection (4.0 mCi/30 mL). Radioactivity levels were assessed at 0.5, 1, 2, 4, and 24 h post-injection and expressed as a percentage of the injected dose per gram (%ID per g) for each organ.

assess the retention characteristics of RESV–^{198}AuNP following a single intratumoral dose of 4 mCi/30 mL directly in SCID mice bearing prostate (PC-3) tumor xenografts and analyzed the radioactivity in the tumors and various organs multiple times (0.5, 1, 2, 4, and 24 h) after euthanizing the animals.

After intratumoral injection, the biodistribution study in PC-3 tumor-bearing SCID mice showed high retention of RESV–^{198}AuNPs in tumor, 252.11 ± 97%ID per g at 0.5 h, which increased to 378.9 ± 60.99%ID per g at 24 h (Fig. 8). There was minimal/no uptake of RESV–^{198}AuNP in other organs, confirming the successful retention of the therapeutic payload at the tumors, with minimal toxic side effects.

Although histopathology and serum biomarker data are not part of this biodistribution-focused report, we believe that the presented evidence provides high tumor selectivity and consistent *in vivo* tolerability, strongly supporting the safe profile of RESV–^{198}AuNP at the administered dose and duration. Additionally, with a short physical half-life of 2.7 days, ^{198}Au decays *via* beta and gamma emission, but the beta energy (~0.96 MeV) is suitable for localized therapeutic effects in tumors without causing systemic irradiation, as evidenced in our extensive investigations and published reports from our group in both mice and dogs.[51–55]

In summary, in the current investigation, animals receiving 136 μCi showed no clinical signs of toxicity, weight loss, behavioral changes, or lethargy during the observation period.

Therapeutic efficacy investigations of RESV–^{198}AuNP

An in-depth assessment was conducted to examine whether RESV–^{198}AuNP could effectively inhibit or decrease tumor volumes in mouse models containing human-derived prostate cancer (PC-3) xenografts. A study was conducted to evaluate the therapeutic efficacy of RESV–^{198}AuNP in treating prostate tumors. Two groups of mice with similar tumor sizes (0.16–0.20 cm^3) and body weights (16.4–24.6 g) were used. The control group received 30 mL of sterile saline, while the treatment group received a single intratumoral injection of RESV–^{198}AuNP (160 mCi/30 mL per tumor). This study lasted 5 weeks post-injection, with day 0 being the randomization day and day 4 being the injection day.

The results demonstrated the tumor-reducing capability of RESV–^{198}AuNP compared to the saline control. Two weeks after treatment (day 14), the RESV–^{198}AuNP group showed a decrease in tumor volume. By week 3 (day 20), the treatment group's tumor volume significantly decreased to 0.10 ± 0.04 cm^3, while the control group's tumor volume doubled to 1.20 ± 0.04 cm^3. Four weeks post-treatment (day 24), the difference was even more pronounced, with the control group's tumor volume (1.40 ± 0.01 cm^3) being ten times larger than the RESV–^{198}AuNPs group (0.14 ± 0.01 cm^3), as shown in Fig. 9.

The tumors in the saline control group appear larger, reflecting the unchecked progression typical of untreated xenografted tumors. Conversely, the tumors in the RESV–^{198}AuNP group are smaller, suggesting that the combination of resveratrol and radioactive gold nanoparticles is effective at suppressing or reducing tumor volume. The most plausible explanation for this difference lies in the dual action of the RESV–^{198}AuNP therapy. Beta radiation emitted by ^{198}Au delivers localized cytotoxic effects to the tumor cells. The resveratrol component sensitizes the tumor by virtue of its antioxidant, anti-inflammatory, and pro-apoptotic properties, thus further enhancing the overall therapeutic impact. Additionally, this nanoparticle formulation benefits from enhanced permeation and retention in the tumor microenvironment, promoting more targeted delivery of both the radioactive isotope and the bioactive resveratrol.

These findings have important implications for future prostate cancer therapies. By co-delivering a radiotherapeutic agent and a compound with established anti-cancer properties,

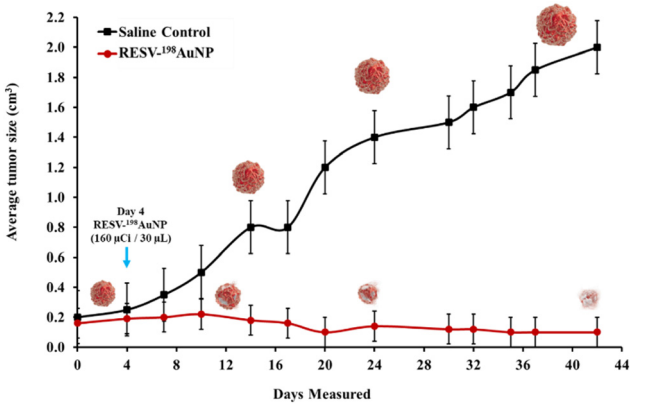

Fig. 9 Tumor volume progression and representative tumor images in mice bearing PC-3 prostate cancer xenografts following treatment with saline (control) and RESV–^{198}AuNPs after single-dose intratumoral administration (mean ± SD). The line graph compares the mean tumor volumes over time for the saline control group (black line) *versus* the RESV–^{198}AuNP group (red line), while the images above illustrate the marked difference in tumor size between the groups at the corresponding time points. The data demonstrate significant inhibition of tumor growth in the RESV–^{198}AuNP-treated mice compared with that in the saline control mice.

RESV–^{198}AuNP presents a promising avenue for reducing systemic side effects while maximizing tumor cell kill. Overall, RESV–^{198}AuNPs demonstrated a reduction in tumor growth in the PC-3 prostate cancer xenograft model, underscoring its potential value as a novel therapeutic strategy for human cancer.

In the context of the present investigation, here, we provide unequivocal evidence that the therapeutic efficacy, as observed and as reported, is solely due to the beta particle emission from radioactive RESV–^{198}AuNP. It is important to note that we used carrier-added RESV–^{198}AuNP as our radioactive gold-198 nanoparticles with an average of 136 μCi for intratumorally delivered therapeutic doses. Through radiochemical calculations, 136 μCi would translate to an equivalent of 136 μg of the non-radioactive RESV–AuNP analog. This concentration of the non-radioactive RES-AuNP does not serve as a control for comparing therapeutic efficacy between the radioactive RESV–^{198}AuNP and the corresponding non-radioactive surrogate RESV–AuNP because at these concentrations of RESV–AuNP, we did not observe any prostate tumor cell death as evaluated through *in vitro* MTT assays. Normally, our animal protocol does not allow therapeutic studies in tumor-bearing mice if the chosen dose range is suboptimal for demonstrating any therapeutic efficacy. With special permission, we performed therapy investigations on just three animals using 136–165 μg of RESV–AuNP. Our results revealed no evidence of therapeutic effects at such low doses of RESV–AuNP. The only educational comparison between radioactive RESV–^{198}AuNP and the corresponding non-radioactive surrogate of RESV–AuNP is to use similar concentrations of the two gold nanoparticles. These observations unequivocally confirm that the therapeutic efficacy, as shown in Fig. 9, is solely due to the beta ray emissions of radioactive gold isotope from RESV–^{198}AuNP. Similar results have been documented through our pioneering investigations published in subsequent leading publications from our laboratory.

Conclusions

RESV–^{198}AuNP represents a significant advancement as a nano-sized radiopharmaceutical with versatile applications in oncology. Its potential as a radiotherapeutic agent for various cancers, including prostate cancer, and as a radiosynovectomy agent underscore its clinical relevance. This study contributes to the growing body of research on a library of biocompatible therapeutic nanoparticles (*e.g.*, Gum Arabic glycoprotein (GA)-functionalized gold-198 nanoparticles (GA^{198}AuNP), epigallocatechin-3-gallate (EGCG)-functionalized gold-198 nanoparticles (EGCG-^{198}AuNP), and mangiferin (MGF)-functionalized gold-198 nanoparticles (MGF-^{198}AuNP)) by demonstrating their safety and efficacy in a cancer treatment modality.

The *in vivo* findings of this study highlight two key aspects: (1) the biocompatibility and non-toxic profile of RESV–^{198}AuNP confirmed through intravenous administration in healthy mice, and (2) the therapeutic potential of RESV–^{198}AuNP validated through intratumoral delivery in prostate (PC-3) tumor-bearing mice. The differential internalization of RESV–AuNP between HAEC endothelial cells and PC-3 prostate cancer cells emphasizes the effectiveness of nanoparticle-based targeting strategies. Leveraging the enhanced permeability and retention (EPR) effect coupled with receptor-mediated uptake/retention, RESV–^{198}AuNP accumulates preferentially in tumor cells, offering a promising platform for precision oncology.

This research highlights the potential of RESV–^{198}AuNP to revolutionize cancer therapy by improving therapeutic outcomes while minimizing systemic toxicity and off-target effects. In addition, this approach overcomes the limitations of brachytherapy by offering a non-surgical technique for administering high doses of therapeutic radiopharmaceutical to the tumor site. Furthermore, the decomposition and decay of the radioactive drug *in vivo* provide additional benefits, including the mechanical removal of seeds used in brachytherapeutic techniques. Functionalizing these nanoparticles with tumor-specific ligands could further enhance their selectivity, sparing healthy tissues and focusing therapeutic action on malignant cells. This study demonstrated the significant therapeutic potential of RESV–^{198}AuNP in treating prostate cancer. The treatment led to a substantial decrease in tumor size compared to the control group, with notable differences observed over time.

The dual action mechanism of RESV–^{198}AuNP contributed to its overall effectiveness. Additionally, RESV–^{198}AuNP holds potential as a theranostic agent, combining imaging capabilities for tumor localization with therapeutic functionalities, such as targeted drug delivery or photothermal therapy. Future research should focus on optimizing nanoparticle functionalization, improving its specificity for tumor cells, and exploring its applications in combinational therapies. With these advancements, RESV–^{198}AuNP could establish a new standard for safer, more effective cancer treatments, offering hope for improved patient outcomes in oncology.

Author contributions

Data curation, formal analysis, investigation, writing – original draft: Tamer M. Sakr, Velaphi C. Thipe, Lisa Watkinson, Terry Carmack; writing – review & editing: Tamer M. Sakr, Velaphi C. Thipe, Kavita K. Katti, Prajna Hegde, Anantkumar Hegde, Ademar B. Lugão; conceptualization, funding acquisition, writing – review & editing: Charles J. Smith, Cathy Cutler, Kattesh V. Katti.

Conflicts of interest

There are no conflicts to declare.

Data availability

The datasets generated and/or analyzed during the current study are available in the article. Additional raw data and any further details supporting the conclusions of this study are available from the corresponding author upon reasonable request.

Acknowledgements

This research was supported by funds from the Kadamba company, Bengaluru, India. We acknowledge the support of IPEN, Sao Paulo, Brazil (Ademar Lugao), and The International Atomic Energy Agency, Austria (IAEA, Tamer Sakr and Kattesh V. Katti). We thank the generous support from Missouri University Research Reactor (MURR), Institute of Green Nanotechnology, University of Missouri (Kattesh V. Katti and Charles J. Smith). The authors gratefully acknowledge the support of the Fulbright Program (Tamer Sakr and Velaphi Thipe: Grant No. 15150089).

References

1 M. Ali, V. Benfante, D. Di Raimondo, G. Salvaggio, A. Tuttolomondo and A. Comelli, Recent Developments in Nanoparticle Formulations for Resveratrol Encapsulation as an Anticancer Agent, *Pharmaceuticals*, 2024, **17**(1), 126, DOI: **10.3390/ph17010126**.

2 S. A. El-Benhawy, M. I. Morsi, E. I. Fahmy, M. A. Soula, F. H. Al Zahraa, F. Khalil and A. R. R. Arab, Role of Resveratrol as Radiosensitizer by Targeting Cancer Stem Cells in Radioresistant Prostate Cancer Cells (PC-3), *Asian Pac. J. Cancer Prev.*, 2021, **22**(12), 3823–3837, DOI: **10.31557/APJCP.2021.22.12.3823**.

3 P. A. Akpa, I. E. Peter and A. M. Onwuka, *et al.*, Nanotheranostics: Platforms, Current Applications, and Mechanisms of Targeting in Breast and Prostate Cancers, *J. Nanotheranostics*, 2023, **4**(3), 346–383, DOI: **10.3390/jnt4030016**.

4 R. Shukla, N. Chanda and A. Zambre, *et al.*, Laminin receptor specific therapeutic gold nanoparticles (198AuNP-EGCg) show efficacy in treating prostate cancer, *Proc. Natl. Acad. Sci. U. S. A.*, 2012, **109**(31), 12426–12431, DOI: **10.1073/pnas.1121174109**.

5 K. V. Katti, M. Khoobchandani and V. C. Thipe, *et al.*, Prostate tumor therapy advances in nuclear medicine: green nanotechnology toward the design of tumor specific radioactive gold nanoparticles, *J. Radioanal. Nucl. Chem.*, 2018, **318**(3), 1737–1747, DOI: **10.1007/s10967-018-6320-4**.

6 M. Khoobchandani, K. K. Katti and A. R. Karikachery, *et al.*, New Approaches in Breast Cancer Therapy Through Green Nanotechnology and Nano-Ayurvedic Medicine - Pre-Clinical and Pilot Human Clinical Investigations, *Int. J. Nanomed.*, 2020, **15**, 181–197, DOI: **10.2147/IJN.S219042**.

7 V. C. Thipe, A. R. Karikachery and P. Çakılkaya, *et al.*, Green nanotechnology—An innovative pathway towards biocompatible and medically relevant gold nanoparticles, *J. Drug Delivery Sci. Technol.*, 2022, **70**, 103256, DOI: **10.1016/j.jddst.2022.103256**.

8 S. Dhoundiyal, S. Srivastava and S. Kumar, *et al.*, Radiopharmaceuticals: navigating the frontier of precision medicine and therapeutic innovation, *Eur. J. Med. Res.*, 2024, **29**(1), 26, DOI: **10.1186/s40001-023-01627-0**.

9 M. R. Papasani, G. Wang and R. A. Hill, Gold nanoparticles: The importance of physiological principles to devise strategies for targeted drug delivery, *Nanomedicine*, 2012, **8**(6), 804–814, DOI: **10.1016/j.nano.2012.01.008**.

10 F. Silva, M. P. Cabral Campello and A. Paulo, Radiolabeled Gold Nanoparticles for Imaging and Therapy of Cancer, *Materials*, 2020, **14**(1), 4, DOI: **10.3390/ma14010004.**.

11 M. S. O. Pijeira, H. Viltres and J. Kozempel, *et al.*, Radiolabeled nanomaterials for biomedical applications: radiopharmacy in the era of nanotechnology, *EJNMMI Radiopharm. Chem.*, 2022, **7**, 8, DOI: **10.1186/s41181-022-00161-4**.

12 V. Thipe, N. Hall and A. Pandurangi, *et al.*, Nano-Ayurvedic Medicine Approaches Using Ginkgo biloba-Phytochemicals Functionalized Gold Nanoparticles Against Breast Cancer, *Nanotechnol., Sci. Appl.*, 2024, **17**, 189–210, DOI: **10.2147/NSA.S478533**.

13 A. H. Ferreira, F. L. N. Marques and C. C. Real, *et al.*, Green Nanotechnology Through Papain Nanoparticles: Preclinical in vitro and in vivo Evaluation of Imaging Triple-Negative Breast Tumors, *Nanotechnol., Sci. Appl.*, 2024, **17**, 211–226, DOI: **10.2147/NSA.S474194**.

14 C. P. Hans, N. Sharma, E. Downey, M. Khoobchandani, K. Katti and K. V. Katti, Mangiferin Conjugated Gold Nanoparticles Protect against the Development of Abdominal Aortic Aneurysm in an Apoe−/− Mouse Model, *JVS Vasc. Sci.*, 2022, 16–17, DOI: **10.1016/j.jvssci.2022.05.038**.

15 M. Khoobchandani, K. Katti, A. Maxwell, W. P. Fay and K. V. Katti, Laminin receptor-avid nanotherapeutic EGCg-AuNPs as a potential alternative therapeutic approach to prevent restenosis, *Int. J. Mol. Sci.*, 2016, **17**(3), 316, DOI: **10.3390/ijms17030316**.

16 N. R. S. Sibuyi, V. C. Thipe and K. Panjtan-Amiri, *et al.*, Green Synthesis of Gold Nanoparticles Using Acai Berry and Elderberry Extracts and Investigation of Their Effect on Prostate and Pancreatic Cancer Cells, *BJGP Open*, 2021, **8**, 1–8, DOI: **10.1177/18495435219953 10**.

17 T. Tangthong, T. Piroonpan and V. C. Thipe, *et al.*, Bombesin peptide conjugated water-soluble chitosan gallate—a new nanopharmaceutical architecture for the rapid one-pot synthesis of prostate tumor targeted gold nanoparticles, *Int. J. Nanomed.*, 2021, **16**, 6957–6981, DOI: **10.2147/IJN.S327045**.

18 M. Khoobchandani, K. K. Katti, A. R. Karikachery, V. C. Thipe, P. L. R. Bloebaum and K. V. Katti, Targeted Phytochemical-Conjugated Gold Nanoparticles in Cancer Treatment, in *Biotechnology Products in Everyday Life*, ed. M. Khoobchandani and A. Saxena, EcoProduction, Springer, Cham, DOI: **10.1007/978-3-319-92399-4_3**.

19 V. C. Thipe, K. P. Amiri and P. Bloebaum, *et al.*, Development of resveratrol-conjugated gold nanoparticles: Interrelationship of increased resveratrol corona on anti-tumor efficacy against breast, pancreatic and prostate cancers, *Int. J. Nanomed.*, 2019, **14**, 4413–4428, DOI: **10.2147/IJN.S204443**.

20 M. Khoobchandani, A. Khan and K. K. Katti, *et al.*, Green nanotechnology of MGF-AuNPs for immunomodulatory intervention in prostate cancer therapy, *Sci. Rep.*, 2021, **11**(1), 16797, DOI: **10.1038/s41598-021-96224-8**.

21 T. Tangthong, T. Piroonpan and V. C. Thipe, *et al.*, Water-Soluble Chitosan Conjugated DOTA-Bombesin Peptide Capped Gold Nanoparticles as a Targeted Therapeutic Agent for Prostate Cancer, *Nanotechnol., Sci. Appl.*, 2021, **14**(14), 69–89, DOI: **10.2147/NSA.S301942**.

22 M. Khoobchandani, K. Katti, A. Zambre and K. V. Katti *Cellular uptake and cytotoxic effects of broccoli phytochemicals based gold nanoparticles (B-AuNPs): Enhanced cancer therapeutic efficacy*. Technical Proceedings of the 2013 NSTI Nanotechnology Conference and Expo, NSTI-Nanotech 2013. 2013; vol. 3: pp. 422–425.

23 K. V. Katti, Realms of green nanotechnology, *Int. J. Green Nanotechnol.*, 2013, **5**(1), 1, DOI: **10.1177/1943089213509648**.

24 V. C. Thipe, A. Jatar, A. R. Karikachery, K. K. Katti and K. V. Katti, Green Nanotechnology of Yucca filamentosa-Phytochemicals-Functionalized Gold Nanoparticles---Antitumor Efficacy Against Prostate and Breast Cancers, *Nanotechnol., Sci. Appl.*, 2023, **16**, 19–40, DOI: **10.2147/NSA.S437812**.

25 N. Daems, C. Michiels, S. Lucas, S. Baatout and A. Aerts, Gold nanoparticles meet medical radionuclides, *Nucl. Med. Biol.*, 2021, **100–101**, 61–90, DOI: **10.1016/j.nucmedbio.2021.06.001**.

26 C. Cutler, P. Kan and N. Chanda, *et al.*, Preparation and use of 198Au/199Au for potential applications in cancer therapy and imaging, *Trans. Am. Nucl. Soc.*, 2010, **103**, 1123–1124.

27 K. V. Katti, M. Khoobchandanai, A. Y. Al-yasiri, K. K. Katti and C. Cutler *Radioactive Gold-198 Nanoparticles In Nanomedicine: Green Nanotechnology and Radiochemical Approaches in Oncology Radioactive Gold-198 Nanoparticles*, In Nanomedicine: Green Nanotechnology and Radiochemical Approaches in Oncology, 2017.

28 N. Chanda, P. Kan and L. D. Watkinson, *et al.*, Radioactive gold nanoparticles in cancer therapy: therapeutic efficacy studies of GA-198AuNP nanoconstruct in prostate tumor-bearing mice, *Nanomedicine*, 2010, **6**(2), 201–209, DOI: **10.1016/j.nano.2009.11.001**.

29 A. Y. Al-Yasiri, M. Khoobchandani and C. S. Cutler, *et al.*, Mangiferin functionalized radioactive gold nanoparticles (MGF-198AuNPs) in prostate tumor therapy: Green nanotechnology for production,: In vivo tumor retention and evaluation of therapeutic efficacy, *Dalton Trans.*, 2017, **46**(42), 14561–14571, DOI: **10.1039/c7dt00383h**.

30 A. R. Jalilian, B. Ocampo-García and W. Pasanphan, *et al.*, IAEA Contribution to Nanosized Targeted Radiopharmaceuticals for Drug Delivery, *Pharmaceutics*, 2022, **14**(5), 1060, DOI: **10.3390/pharmaceutics14051060**.

31 B. Ocampo-García, B. Gibbens-Bandala, E. Morales-Avila, *et al.*, *Dual-Targeted Therapy and Molecular Imaging with Radiolabeled Nanoparticles*, Springer International Publishing, 2019, DOI: **10.1007/978-3-319-92399-4_14**.

32 J. J. Santos, J. Leal and L. A. P. Dias, *et al.*, Bovine Serum Albumin Conjugated Gold-198 Nanoparticles as Model To Evaluate Damage Caused by Ionizing Radiation to Biomolecules, *ACS Appl. Nano Mater.*, 2018, **1**(9), 5062–5070, DOI: **10.1021/acsanm.8b01174**.

33 K. V. Katti, Renaissance of nuclear medicine through green nanotechnology: functionalized radioactive gold nanoparticles in cancer therapy—my journey from chemistry to saving human lives, *J. Radioanal. Nucl. Chem.*, 2016, **309**(1), 5–14, DOI: **10.1007/s10967-016-4888-0**.

34 F. Concurrent, M. Imaging, T. Therapy, K. V. Katti, K. K. Katti and M. Khoobchandani *Radioactive Gold Nanoparticles with Beta Energy and Auger Electron Cascades*, In Nanomedicine: Green Nanotechnology and Radiochemical, *Published online* 2018.

35 V. Kattumuri, K. Katti and S. Bhaskaran, *et al.*, Gum arabic as a phytochemical construct for the stabilization of gold nanoparticles: In vivo pharmacokinetics and X-ray-contrast-imaging studies, *Small*, 2007, **3**(2), 333–341, DOI: **10.1002/smll.200600427**.

36 R. Kannan, A. Zambre and N. Chanda, *et al.*, Functionalized radioactive gold nanoparticles in tumor therapy, *Wiley Interdiscip. Rev.: Nanomed. Nanobiotechnol.*, 2012, **4**(1), 42–51, DOI: **10.1002/wnan.161**.

37 R. Kannan, V. Rahing and C. Cutler, *et al.*, Nanocompatible chemistry toward fabrication of target-specific gold nanoparticles, *J. Am. Chem. Soc.*, 2006, **128**(35), 11342–11343, DOI: **10.1021/ja063280c**.

38 B. Seniwal, L. F. De Freitas, V. C. Thipe and S. Singh *Brachytherapy using radioactive nanoparticles: an alternative to seed based brachytherapy*. *Published online* 2020, pp. 1–19.

39 C. Cutler, A. Al-Yasiri and M. Kuchuk, *et al.*, Comparison of in vivo uptake of radioactive gold nanoparticles formulated using phytochemicals, *J. Nucl. Med.*, 2015, **56**(supplement 3), 1267 LP-1267. **https://jnm.snmjournals.org/content/56/supplement_3/1267.abstract**.

40 J. Katrin Badawi *Review Article Resveratrol Used as Nanotherapeutic: A Promising Additional Therapeutic Tool against Hormone-Sensitive, Hormone-Insensitive and Resistant Prostate Cancer*, 2023, **11**. **https://www.ajceu.us/**.

41 S. Ganapathy, Q. Chen, K. P. Singh, S. Shankar and R. K. Srivastava, Resveratrol enhances antitumor activity of TRAIL in prostate cancer xenografts through activation of FOXO transcription factor, *PLoS One*, 2010, **5**(12), e15627, DOI: **10.1371/journal.pone.0015627**.

42 M. Farhan, Cytotoxic Activity of the Red Grape Polyphenol Resveratrol against Human Prostate Cancer Cells: A Molecular Mechanism Mediated by Mobilization of Nuclear Copper and Generation of Reactive Oxygen Species, *Life*, 2024, **14**(5), 611, DOI: **10.3390/life14050611**.

43 Z. Faisal, A. Mazhar and S. A. Batool, *et al.*, Exploring the multimodal health-promoting properties of resveratrol: A comprehensive review, *Food Sci. Nutr.*, 2024, **12**(4), 2240–2258, DOI: **10.1002/fsn3.3933**.

44 A. S. Choudhari, P. C. Mandave, M. Deshpande, P. Ranjekar and O. Prakash, Phytochemicals in cancer treatment: From preclinical studies to clinical practice, *Front. Pharmacol.*, 2020, **10**, 1614, DOI: **10.3389/fphar.2019.01614**.

45 D. S. Han, H. J. Lee and E. O. Lee, Resveratrol suppresses serum-induced vasculogenic mimicry through impairing the EphA2/twist-VE-cadherin/AKT pathway in human prostate cancer PC-3 cells, *Sci. Rep.*, 2022, **12**, 20125, DOI: **10.1038/s41598-022-24414-z**.

46 N. M. Saad, M. Sekar, S. H. Gan, P. T. Lum, J. Vaijanathappa and S. Ravi, Resveratrol: Latest scientific evidences of its chemical, biological activities and therapeutic potentials, *Pharmacogn. J.*, 2020, **12**(6), 1779–1791, DOI: **10.5530/pj.2020.12.240**.

47 M. Annaji, I. Poudel, S. H. S. Boddu, R. D. Arnold, A. K. Tiwari and R. J. Babu, Resveratrol-loaded nanomedicines for cancer applications, *Cancer Rep.*, 2021, **4**(3), e1353, DOI: 10.1002/cnr2.1353.

48 T. Dixit, N. Dave, K. Basu, P. Sonawane, T. Gawas and S. Ravindran, Nano-radiopharmaceuticals as therapeutic agents, *Front. Med.*, 2024, **11**, 1355058, DOI: 10.3389/fmed.2024.1355058.

49 Y. Fang, V. G. Demarco and M. B. Nicholl, Resveratrol enhances radiation sensitivity in prostate cancer by inhibiting cell proliferation and promoting cell senescence and apoptosis, *Cancer Sci.*, 2012, **103**(6), 1090–1098, DOI: 10.1111/j.1349-7006.2012.02272.x.

50 A. A. Arabzadeh, T. Mortezazadeh, T. Aryafar, E. Gharepapagh, M. Majdaeen and B. Farhood, Therapeutic potentials of resveratrol in combination with radiotherapy and chemotherapy during glioblastoma treatment: a mechanistic review, *Cancer Cell Int.*, 2021, **21**(1), 391, DOI: 10.1186/s12935-021-02099-0.

51 N. Chanda, A. Upendran and E. J. Boote, *et al.*, Gold nanoparticle based X-ray contrast agent for tumor imaging in mice and dog: A potential nano-platform for computer tomography theranostics, *J. Biomed. Nanotechnol.*, 2014, **10**(3), 383–392, DOI: 10.1166/jbn.2014.1725.

52 S. M. Axiak-Bechtel, A. Upendran and J. C. Lattimer, *et al.*, Gum arabic-coated radioactive gold nanoparticles cause no short-term local or systemic toxicity in the clinically relevant canine model of prostate cancer, *Int. J. Nanomed.*, 2014, **9**, 5001–5011, DOI: 10.2147/IJN.S67333.

53 G. M. Fent, S. W. Casteel and D. Y. Kim, *et al.*, Biodistribution of maltose and gum arabic hybrid gold nanoparticles after intravenous injection in juvenile swine, *Nanomedicine*, 2009, **5**(2), 128–135, DOI: 10.1016/j.nano.2009.01.007.

54 E. Boote, G. Fent and V. Kattumuri, *et al.*, Gold Nanoparticle Contrast in a Phantom and Juvenile Swine: Models for Molecular Imaging of Human Organs using X-ray Computed Tomography, *Acad. Radiol.*, 2010, **17**(4), 410–417, DOI: 10.1016/j.acra.2010.01.006.

55 N. Chanda, V. Kattumuri and R. Shukla, *et al.*, Bombesin functionalized gold nanoparticles show in vitro and in vivo cancer receptor specificity, *Proc. Natl. Acad. Sci. U. S. A.*, 2010, **107**(19), 8760–8765, DOI: 10.1073/pnas.1002143107.

